

MACIEJ DWORNIK  
ANNA FRANCZYK  
ANDRZEJ LEŚNIAK  
KRZYSZTOF KRAWIEC

## INFLUENCE OF INITIAL WATER SATURATION IN EARTHEN LEVEES ON RESULTS OF NUMERICAL MODELLING OF INFILTRATION PROCESSES

**Abstract** *Levees in Poland are mostly earthen constructions. The stability of earthen levees depends largely on factors such as the construction material, meteorological conditions, and natural elements. The influence of the initial water saturation of the pore space on levee stability is analyzed in this paper. The analysis was performed using numerical modeling, and the water pore-pressure results were compared to the data obtained from the sensors located in a levee. The numerical modeling shows a moderate influence of the initial water level on the distribution of water pore pressure during high water levels. The influence of the initial water level in a levee is the smallest in the infiltration zone close to water reservoir and increases with distance from the water.*

**Keywords** water saturation, numerical modeling, levee

**Citation** Computer Science 18(4) 2017: 413–427

## 1. Introduction

Levees in Poland are mostly earthen constructions. Human life and property very often depend on the state of these constructions. The stability of earthen levees depends largely on factors such as the construction material, meteorological conditions (precipitation), and natural elements (vegetation, burrowing animals, topography, or hydrological condition of area).

The influence of the initial water saturation of a pore space (open space in the rock or soils) on levee stability is analyzed in this paper. An analysis was performed using numerical modeling, and the water pore-pressure results were compared to the data obtained from the sensors located in a levee. The water saturation of a pore space in a levee depends on several factors, such as precipitation, drainage capability of the levee, and water level of the river, sea, or reservoir before a high water level occurs. A high saturation of the pore space significantly decreases the stability of earthen constructions and increases the probability of levee failure (i.e., [10, 16]).

Four initial saturations of levee pore space were assumed:

1. completely dry levee;
2. height of full water saturation equal to 1/6 of levee height;
3. height of full water saturation equal to 1/3 of levee height;
4. height of full water saturation based on sensor measurements.

There are no dense pore pressure sensor networks in the levees on Polish rivers; therefore, in lieu of real measurements, the possibility of using the theoretical initial water saturation presented above was tested. This hypothesis was tested for two different flood-wave scenarios, and the results were compared to the sensor measurements of water pore pressure from inside levees. The influence of the initial water saturation was tested using numerical modeling in Itasca FLAC 7.0 2D software.

The results presented in this paper were conducted as part of the ISMOP Project [9], during which an earthen flood embankment in the shape of a stadium was built and used for the simulation of flood waves by changing the water level in the internal reservoir. A dense network of sensors (water pore pressure, temperature, strain, piezometers) was placed inside this construction [1]. An early warning computer system based on these measurements will be created as part of the ISMOP Project ([3, 6]). The IJkdijk and Urbanflood projects were similar in that they used artificial and natural constructions to conduct the experiments ([7, 14, 11]).

## 2. Theory

FLAC (Fast Lagrangian Analysis of Continua) is a two-dimensional, explicit, finite difference program that performs lagrangian analysis for the computation of engineering mechanics. The numerical formulation in FLAC is conceptually similar to that of dynamic relaxation [13] with the adoption of difference equations for grid elements of any shape [15], large strains, and varying damping.

FLAC uses dynamic equations of motion even for static problems. The explicit calculation sequence in FLAC is illustrated in Figure 1.

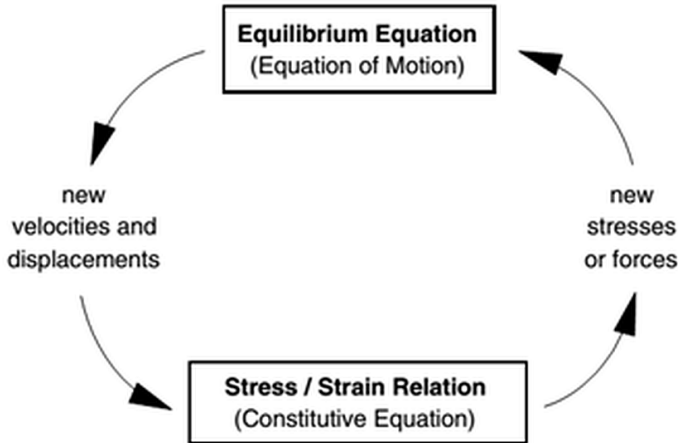


**Figure 1.** Explicit calculation sequence in FLAC [8].

The calculation procedure first solves the equation of motion to find new velocities and displacements from stresses and forces. In the next step, strain rates are derived from the velocities and new stresses from the strain rates. In each box in the scheme above, grid variables are updated in an explicit way from the known values that remain fixed within the box. A short time step is chosen to prevent numerical errors.

FLAC makes it possible to update the grid coordinates at each time step in the large-strain mode in terms of Lagrangian formulation; this is in contrast to an Eulerian formulation, in which the material moves and deforms relative to a fixed grid.

In this work, we prepared a model of the flow of fluid through a permeable levee with mechanical interaction. One type of fluid – solid interaction is consolidation, in which the slow dissipation of pore pressure causes displacements to occur in the soil. This type of behavior involves two mechanical effects. First, changes in pore pressure cause changes in the effective stress, which affect the response of the solid. Second, the fluid in a zone reacts to mechanical volume changes by a change in pore pressure [8].

The numerical formulation of coupled fluid-mechanical processes is based on the quasi-static Biot theory and is applied to problems concerning single-phase Darcy flow in a porous medium. The Darcy law concerns water filtration in a saturation zone. A generalization of this law for an aeration zone is represented by the Richards equation.

Fluid flow is characterized by Darcy's law (eq. 1):

$$q_i = -k_{ij} \hat{k}(s) \frac{\partial}{\partial x_j} (P - \rho_w g_k x_k) \quad (1)$$

where:

- $q_i$  – specific discharge vector,
- $k_{ij}$  – mobility coefficient,
- $\hat{k}(s)$  – relative permeability (which is a function of the saturation  $s$ ),
- $P$  – fluid pore pressure,
- $\rho_w$  – mass density of the fluid,
- $g_i$  – two components of the gravity vector (for  $i = 1, 2$ ).

The changes in pore pressure caused changes in the effective stresses:

$$\sigma'_{ij} = \sigma_{ij} + \alpha P \delta_{ij} \quad (2)$$

where  $\alpha$  is Biot's effective stress parameter [8].

The incremental stress and strain during a time step is governed by various elastic or elasto-plastic constitutive laws, which can be written in a general form as:

$$\frac{\partial \sigma'_{ij}}{\partial t} = H(\sigma'_{ij}, \epsilon'_{ij}, k) \quad (3)$$

in which  $H$  contains the given material functions,  $\epsilon'_{ij}$  is the infinitesimal strain-rate tensor, and  $\partial t$  is a time increment. Numerical simulations were carried out under plane-strain conditions using the Mohr-Coulomb failure criterion. This criteria requires us to declare five parameters: density  $\rho$ , internal friction angle  $\varphi$ , cohesion  $c$ , bulk modulus  $K$ , and shear modulus  $G$ .

The equations mentioned above are solved in terms of the finite difference method after discretization of the model into quadrilateral elements. FLAC uses an explicit method to solve the algebraic equations. For such a simulation, assumptions of the small time step are necessary in order to ensure the stability of the numerical solution. As the system is required to always be in mechanical equilibrium, the time-dependent stress increment must not be large as compared to the strain-dependent stress increment. In the case of the fluid flow calculations, the time step depends on the smallest zone size and fluid diffusivity [8].

### 3. Numerical modeling

The numerical model was generated using a squared mesh with a cell size of 0.1 m  $\times$  0.1 m (Fig. 2). Several bounding conditions were applied. For the mechanical calculations on the bottom edge (depth = 3 m), the Dirichlet boundary condition was applied. The displacements and velocities in both directions were fixed to zero.

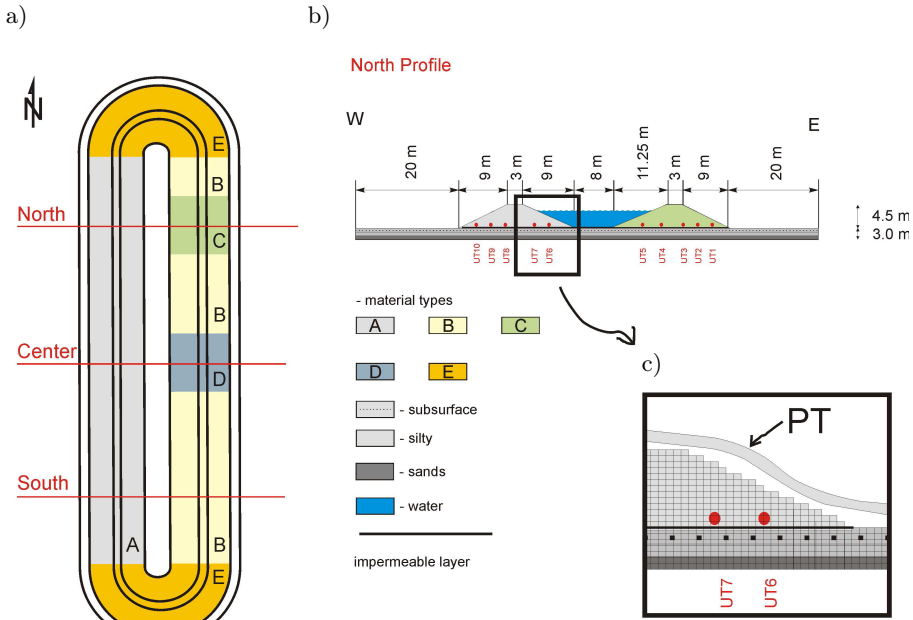


**Figure 2.** Shape of levee (a) with location of water pore-pressure sensors in north cross section (b) and assumed computational mesh (c). With wide line, boundary conditions for pore pressure (P) and temperature (T) for all surface nodes were depicted.

On the left and right edges (20 m from the levee’s edge), the displacements and velocities were fixed to a zero value only in the horizontal direction. For the fluid-flow calculations, pore-pressure values were fixed only on the upper edge of the model and depended on their locations (contact with air or water) and actual water level in the internal reservoir. The water levels and pore pressures were updated at 1h intervals during the simulation. All of the values of the geomechanic and fluid-flow parameters used in the numerical modeling are presented in Table 1.

**Table 1**  
Values of parameters used in numerical modeling [2, 12].

	NW levee	NE levee	Subsurface	Silty	Sands
Density $\rho$ [g/cm <sup>3</sup> ]	1.90	1.96	2.10	1.89	1.85
Cohesion $c$ [KPa]	12.50	15.43	10.30	13.70	10.00
Friction $\varphi$ [°]	30.04	35.20	32.90	22.50	36.20
Bulk Modulus $K$ [MPa]	8.53	7.25	7.25	16.20	36.30
Shear Modulus $G$ [MPa]	3.27	3.35	3.43	6.63	21.80
Porosity $n$ [%]	37	32	27	40	35
Mobility coefficient $k$ [m/s]	1.83E-5	5.24E-5	1.52E-5	1.35E-5	5.60E-6

Numerical modeling of the flood was always performed after double calculations of mechanical equilibrium: first, only for the geological medium; and second, for the whole model (geological medium and levee). Subsequently, fluid flows were simulated. After each 1h of simulation, the mechanical equilibrium was calculated. This time step is short enough for a correct simulation of the flooding phenomena. A shorter time step increased calculation time but did not offer any significant advantages. A detailed description of the numerical calculation can be found in [4] or [5].

Four schemes of initial water saturation of pore space in the levee were assumed (Fig. 3):

1. levee completely dry;
2. height of full water saturation equal to 1/6 of levee height;
3. height of full water saturation equal to 1/3 of levee height;
4. height of full water saturation based on sensor measurements; in this case, the nearest neighbor interpolation method was used to determine the water saturation level; after a few time steps, the fluid state equilibrium was obtained; this method was faster than the linear method to initialize the water saturation of the pore space.

The highest value of the initial water saturation equal to 1/3 of the levee height was assumed after analysis of the water-level measurements before and a few days after the real experiments were conducted.

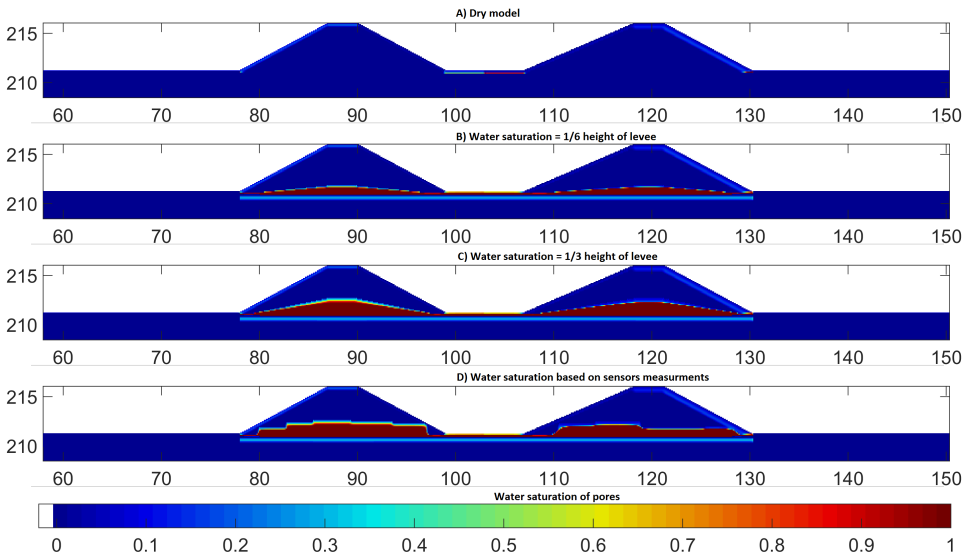


**Figure 3.** Initial water saturation of pore space in levee for 4 m experiment. White stars on Part D) corresponds to localization of water pore-pressure sensors.

The water saturation schemes shown above were tested for two different flooding scenarios (Fig. 4). The experiments were conducted between the 29<sup>th</sup> of August and 09<sup>th</sup> of September, 2016, for the 3 m flood wave and between the 13<sup>th</sup> and 22<sup>nd</sup> of September, 2016, for the 4 m flood wave.

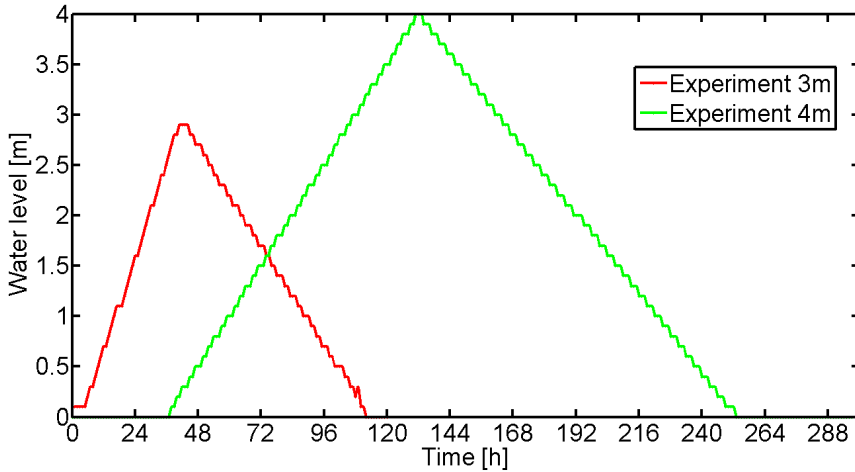


**Figure 4.** Scenario of changing water levels inside water reservoir based on real measurements.

## 4. Results

The results of the numerical modeling are presented in Figures 5 and 6 for the 4 m experiment. The distributions of water pore pressure are presented for two time moments:

- after 133 h, at maximum water level (Fig. 5);
- after 255 h, when flood wave decreased to zero level (Fig. 6).

Differences between the initial saturation models were mainly visible in the area just above the impermeable layer in the external wings of the levees. The modeled pore-pressure distributions are very similar, with the exception of the dry model (Fig. 5A). In the infiltration zone, the shape and values of the pore-pressure isolines were similar for all models of the initial water saturation of the pore space (Fig. 5). After the flood wave had ended (255 h, Fig. 6), there were almost no differences between the initial water saturation models.

The 3 m experiment had similar conclusions to the 4 m experiment, with the most-visible differences being outside the infiltration zone. In these areas, water saturation in the pore space was similar to the initial pore-pressure values. In the infiltration zone, the initial differences were reduced by water flow in the pore space of the levee.

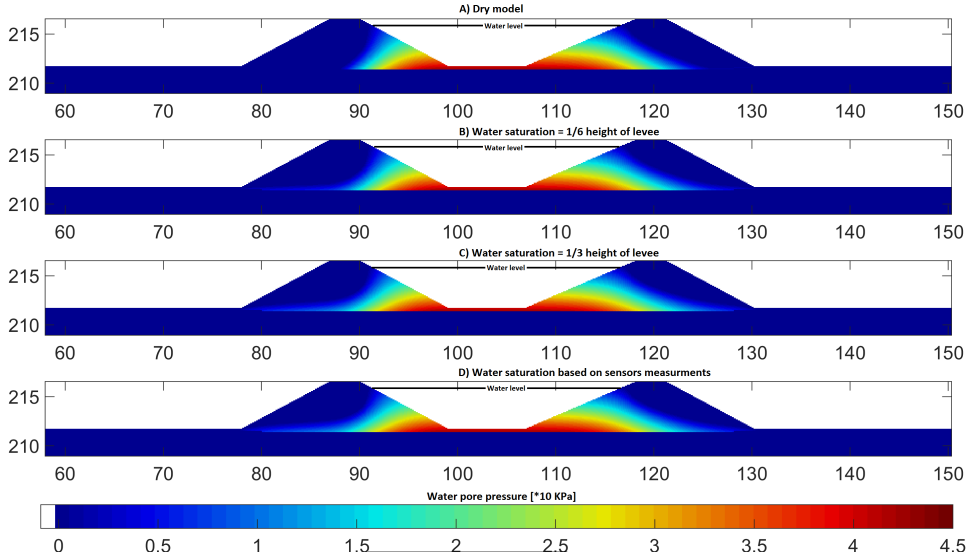


**Figure 5.** Distribution of water pore pressure (\*10 KPa) for initial water saturation in levee for maximum water level in reservoir for 4 m experiment. Simulation results after 133 h.

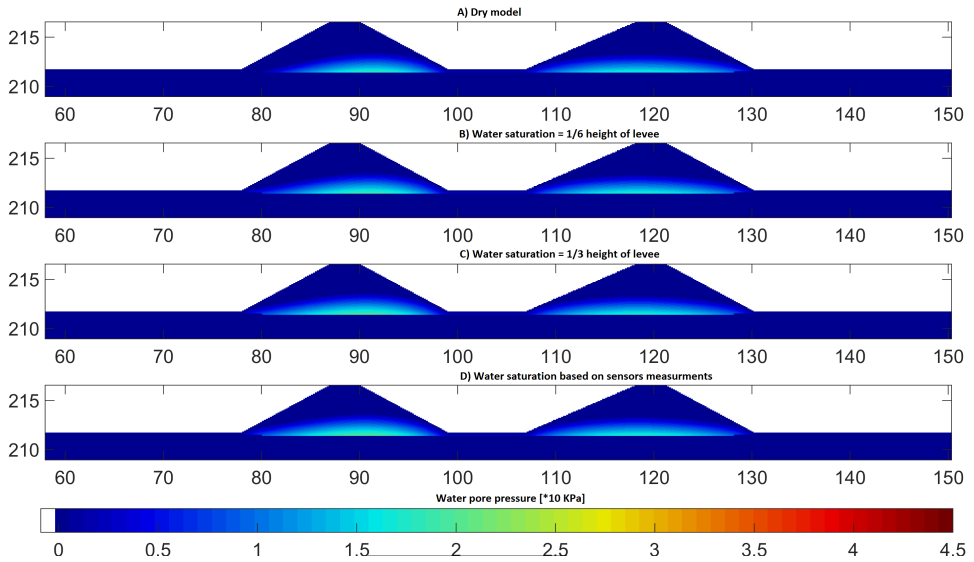


**Figure 6.** Distribution of water pore pressure [\*10 KPa] after 255 h (0 m water level in reservoir) for 4 m experiment.

The results obtained from the sensors in the experimental 4 m levee during the flooding experiment together with the results of the numerical modelings are presented in Figure 7. Sensors ut5 and ut6, which were placed nearest to the water side of the embankment, measured the highest pore-pressure values. The greater the distance between the sensor and the embankment’s water side, the lower the pore-pressure values observed (ut9, ut10, ut1 and ut2). In addition, for most of the sensors, a high compatibility is achieved between the measured and modeled pore-pressure values in defining the time interval when the dynamic changes within the embankment start (arrows in Figure 7 for plots ut1 – ut8).

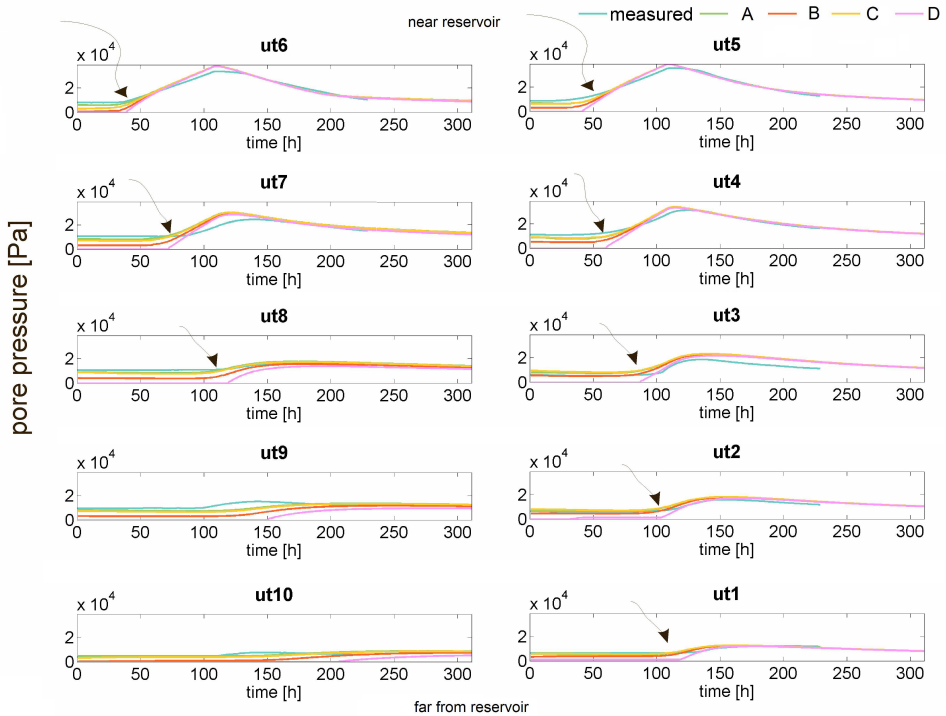


**Figure 7.** Sensor readings obtained during 4 m flood-wave experiment (blue line) together with values computed during numerical calculation for initial saturation that corresponds to real measurements (green line); zero saturation (purple line); and saturation assumed as 1/3 and 1/6 of levee height (red and yellow lines, respectively).

Results of the 3 m experiment presented the same good agreement between the measured and modeled data. The plots of the maximum pore-pressure values and the times of occurrence obtained from the sensors and in the numerical modeling of the flood wave with different initial saturation levels are presented in Figure 8.

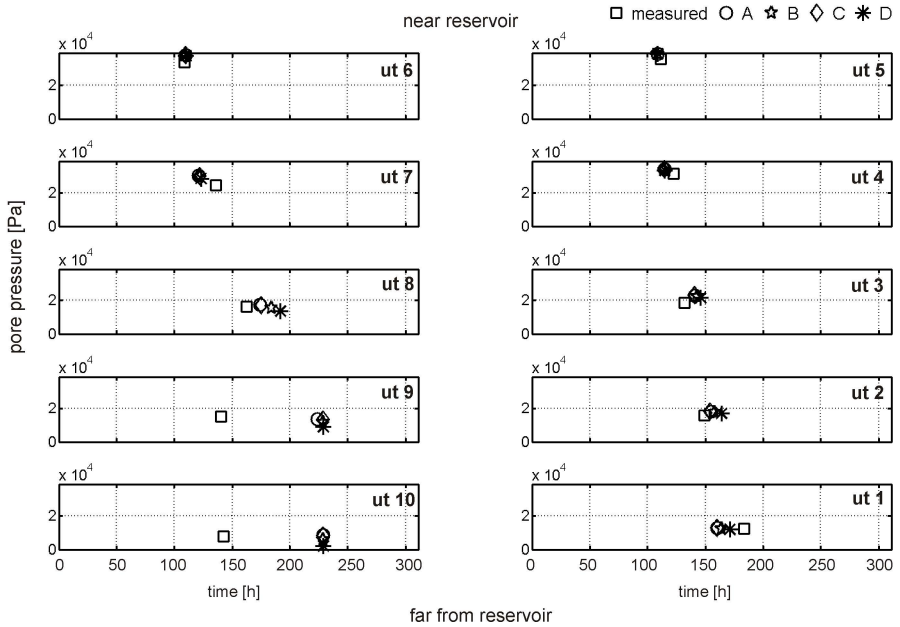


**Figure 8.** Maximum pore-pressure values and time of occurrence obtained during 4 m flood-wave experiment (marked with square) together with values computed during numerical calculation for initial saturation which corresponds to real measurements (Model A – marked with circle); zero saturation (Model B – marked with pentagram); and saturation assumed as 1/3 and 1/6 of levee height (Models C and D – marked with diamond and asterisk, respectively).

The best consistency of maximum pore-pressure value and time of occurrence among the modeled and recorded data were obtained for the sensors located on the water side of the embankment (ut4 – ut7). When the distance from the embankment water side was increased, the maximum values of pore pressure in all of the presented plots decreased. Increasing the distance between the sensors and the water side of the embankment also caused the maximum pore-pressure value to occur later. For sensors on the east side of the experimental embankment (ut1 – ut5), the maximum pore pressure occurs earlier than for the sensors located on the west side of the embankment (ut6 – ut10). The times at which the maximum pore pressure occurred varied due to the difference in the permeability of the material on both sides of the embankment levee (Tab. 1). This relationship is not maintained for the data measured by sensors ut9 and ut10 during the real flood-wave experiment. The time of the maximum value of pore pressure measured by sensors ut9 and ut10 is shorter than the time measured by sensor ut8, which is placed closer to the flooding wave. These measurements are due to the local weakening of the embankment area where a small leakage was observed in a later experiment.

The same conclusion about the maximum pore-pressure value and time of occurrence in both the modeled and recorded data is also valid for the the 3 m experiment (Fig. 9). There is a lack of information from sensors ut9 and ut10, because these sensors did not measure any saturation nor was any saturation calculated during the numerical modeling. The difference for sensor ut1 between the occurrence time of the measured data and the modeled data is related to a faulty measurement in this position.

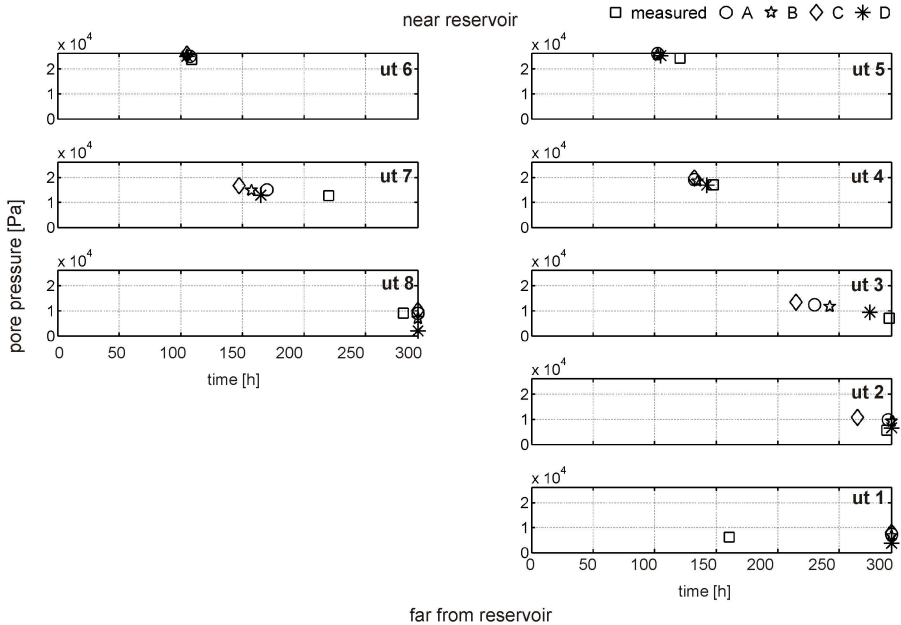


**Figure 9.** Maximum pore-pressure values and time of occurrence obtained during 3 m flood-wave experiment (marked with square) together with values computed during numerical calculation for initial saturation, which corresponds to real measurements (Model A – marked with circle); zero saturation (Model B – marked with pentagram); and saturation assumed as 1/3 and 1/6 of levee height (Models C and D – marked with diamond and asterisk, respectively).

Figure 10 shows the RMS differences between the data measured during the flood-wave experiment and the data obtained from the numerical modeling. The RMS values were computed for all sensor locations for all recorded or modeled time intervals and for the time intervals after the dynamic changes occurred. The RMS values were computed for the data normalized to the maximum value obtained during measurement and numerical calculation. RMS difference plots obtained for the 3 m experiment confirm the good compatibility of the measured and modeled data achieved in the area of the dynamic changes (Fig. 11).

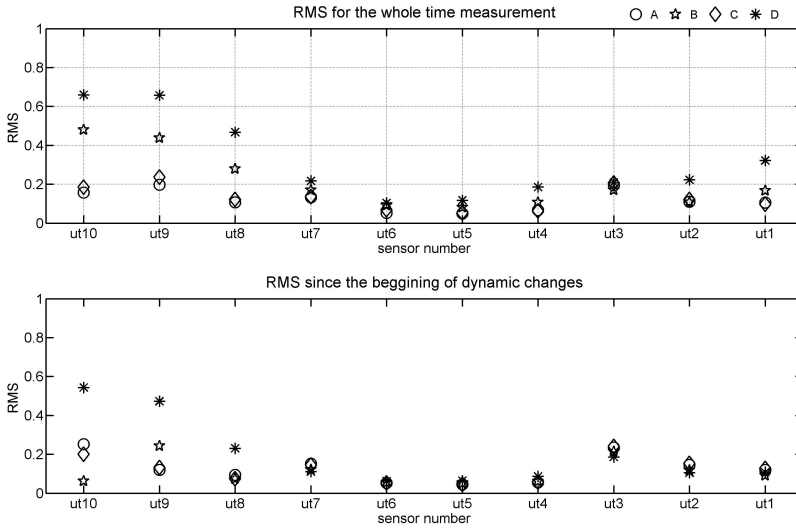


**Figure 10.** RMS differences between data measured during 4 m flood-wave experiment and data obtained from numerical modeling for initial saturation, which corresponds to real measurements (Model A – marked with circle); zero saturation (Model B – marked with pentagram); and saturation assumed as 1/3 and 1/6 of levee height (Models C and D – marked with diamond and asterisk, respectively).

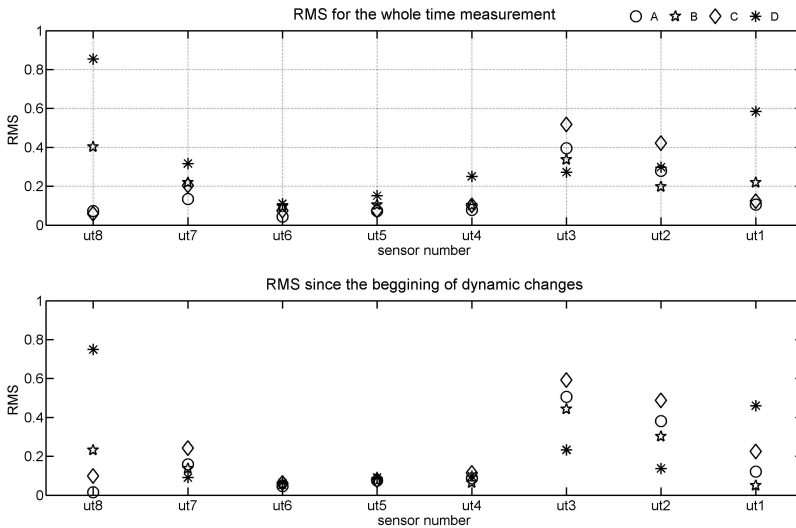


**Figure 11.** RMS differences between data measured during 3 m flood-wave experiment and data obtained from numerical modeling for initial saturation, which corresponds to real measurements (Model A – marked with circle); zero saturation (Model B – marked with pentagram); and saturation assumed as 1/3 and 1/6 of levee height (Models C and D – marked with diamond and asterisk, respectively).

## 5. Conclusions

The numerical modeling shows the moderate influence of the initial water level on the distribution of water pore pressure during high water levels. In the region of the dynamic changes where the water inflow is observed, the changes in the water levels are mutually similar. On the other side of the embankment (where there was no water infiltration), the differences between the pore pressures depend only on the assumed initial values of the pore pressures; the exception is the model where the embankment was initially dry. In that case, the pore-pressure values are remarkably different from those observed in the models with “wet” initial conditions. Another conclusion that can easily be seen from the modeling is that the particular course of flooding and maximum water level have no direct influence on the water-saturation changes. A far-more-important factor in terms of the results of the numerical modeling is the assumed geotechnical parameters and shape and size of the embankment, as well as the particular “scenario” of flooding realized during the modeling.

The parts of the earthen embankments that face hazardous phenomena such as water leakage and loss of cohesion are located in the regions of strong dynamic changes. The results obtained from the modeling show that a lack of pore-pressure measurements and only a rough approximation of the initial pore-pressure conditions do not have a major impact on the model correctness and results in a region. It is most important not to assume unrealistic, completely dry conditions that result in large differences between the synthetic and real measurement data. This conclusion is important because there is almost no field monitoring of pore pressure conducted in the Polish river embankment system. Hence, we can state that a lack of measurements does not preclude a successful prediction of the infiltration processes and stability supervision of embankments.

## Acknowledgements

*This work is financed by the National Center for Research and Development (NCBiR), Poland, project PBS1/B9/18/2013 – (no 180535). This work was partly supported by AGH University of Science and Technology, Faculty of Geology, Geophysics and Environmental Protection, as a part of a statutory research project.*

## References

- [1] Balis B., Brzoza-Woch R., Bubak M., Kasztelnik M., Kwolek B., Nawrocki P., Nowakowski P., Szydło T., Zielinski K.: Holistic approach to management of IT infrastructure for environmental monitoring and decision support systems with urgent computing capabilities, *Future Generation Computer Systems*, vol. 79(1), pp. 128–143, 2018.

- [2] Borecka A., Kaczmarczyk R., Krokoszyński P., Ptaszek M., Stanisz J., Korzec K., Kret E., Tchórzewska S., Nowak P., Świątek M., Pękała M., Dąbrowski J.: Dokumentacja geologiczno-inżynierska wraz z dokumentacją badań podłoża gruntowego sporządzona w celu określenia warunków geologiczno-inżynierskich dla projektowanej budowy eksperymentalnego wału przeciwpowodziowego na działce nr 796 w Czernichowie, 2014.
- [3] Brzoza-Woch R., Konieczny M., Kwolak B., Nawrocki P., Szydło T., Zieliński K.: Holistic approach to urgent computing for flood decision support, *Procedia Computer Science*, vol. 51, pp. 2287–2396, 2015.
- [4] Dwornik M., Krawiec K., Pięta A., Leśniak A.: Numerical and experimental stability analysis of earthen levees. In: *IAMG 2015: the 17th annual conference of the International Association for Mathematical Geosciences: Freiberg, Germany*, September 5–13, 2015, vol. AMG 2015, pp. 857–864, 2015.
- [5] Dwornik M., Pieta A., Bala J.: Numerical modelling of temperature and pore pressure distribution in the embankment during flooding processes, *SGEM 2015: Science and Technologies in Geology, Exploration and Mining*, vol. 2, pp. 479–496, 2015.
- [6] Habrat M., Lupa M., Chuchro M., Leśniak A.: A decision support system for emergency flood embankment stability, *Procedia Computer Science*, vol. 51, pp. 2957–2961, 2015.
- [7] IJkdijk: project website. [www.ijkdijk.eu](http://www.ijkdijk.eu).
- [8] Inc. I.C.G.: FLAC – User Manual, 2007. Minneapolis.
- [9] ISMOP: project website. <http://www.ismop.edu.pl>.
- [10] Iverson R.: Landslide triggering by rain infiltration, *Water Resources Research*, vol. 36(7), pp. 1897–1910, 2000.
- [11] Melnikova N., Krzhizhanowskaya V., Sloot P.: Modeling earthen dikes using real-time sensor data, *Journal of Hydrology*, vol. 496, pp. 154–165, 2013.
- [12] Mościcki J., Bania G., Ćwiklik M., Borecka A.: DC resistivity studies of shallow geology in the vicinity of Vistula River flood bank in Czernichów Village (near Kraków in Poland), *Studia Geotechnica et Mechanica*, vol. 36(1), pp. 63–70, 2014.
- [13] Otter J.R.H., Cassell A.C., Hobbs R.E.: Dynamic Relaxation (Paper No. 6986), *Proceedings of the Institution of Civil Engineers*, vol. 35, pp. 633–656, 1966.
- [14] UrbanFlood: project website. <http://www.urbanflood.eu>.
- [15] Wilkins M.: *Methods in Computational Physics*, vol. 3, chap. Fundamental Methods in Hydrodynamics, pp. 211–263, 1964.
- [16] Xue K., Ajmera B., Tiwari B., Hu Y.: Effect of long duration rainstorm on stability of Red-clay slopes, *Geoenvironmental Disasters*, vol. 3(12), pp. 1–13, 2016.

## **Affiliations**

### **Maciej Dwornik**

AGH University of Science and Technology, Faculty of Geology, Geophysics and Environmental Protection, al. Adama Mickiewicza 30, 30-059 Kraków,  
dwornik@geol.agh.edu.pl

### **Anna Franczyk**

AGH University of Science and Technology, Faculty of Geology, Geophysics and Environmental Protection, al. Adama Mickiewicza 30, 30-059 Kraków

### **Andrzej Leśniak**

AGH University of Science and Technology, Faculty of Geology, Geophysics and Environmental Protection, al. Adama Mickiewicza 30, 30-059 Kraków

### **Krzysztof Krawiec**

The Mineral and Energy Economy Research Institute of the Polish Academy of Sciences,  
ul. Józefa Wybickiego 7, 31-261 Kraków

**Received:** 31.12.2016

**Revised:** 01.06.2017

**Accepted:** 28.07.2017